

Silicon Carbide Nanosprings

Daqing Zhang,* Abdullah Alkhateeb, Hongmei Han, Hasan Mahmood, and David N. McIlroy

Department of Physics, University of Idaho, Moscow, Idaho 83844-0903

M. Grant Norton

School of Mechanical and Materials Engineering, Washington State University, Pullman, Washington 99164-2920

Received May 6, 2003; Revised Manuscript Received May 15, 2003

ABSTRACT

Amorphous silicon carbide nanosprings, as well as biphas (crystalline core/amorphous sheath) helical nanowires, have been synthesized by plasma enhanced chemical vapor deposition. Both variants grow via the vapor–liquid–solid mechanism. The formation of the amorphous silicon carbide nanosprings is explained in terms of the contact angle anisotropy model initially proposed to explain the formation of amorphous boron carbide nanosprings. A modified contact angle anisotropy model, where the presence of temperature gradients within the catalyst are imposed, has been proposed to explain the formation of the biphas helical nanowires. The basis for this model is that the crystalline core acts to pin the catalyst, thereby prohibiting nanospring formation. The model is supported by the experimental observation of a transition to nanospring growth at the point of extinction of the crystalline core of a linear biphas nanowire at a position where the catalyst is off-center with respect to the axis of the growth direction.

One-dimensional nanowires are attracting increased attention from the scientific and technological communities because of their versatile electrical, optical, and mechanical properties.^{1–6} Potential applications for these novel structures range from tips in scanning probe microscopes to interconnects in nanoelectrical devices as well as the utilization of their field-emission properties in flat-panel displays.^{7–9} Silicon carbide (SiC) is a particularly attractive material for these applications because of its high thermal and electric conductivities and outstanding mechanical properties.⁸ Several groups have successfully synthesized SiC nanowires (or nanorods) by a variety of techniques.^{10–13} For example, Dai et al. prepared SiC nanorods through a reaction between carbon nanotubes and SiO or SiI₂,¹⁰ and Meng and co-workers fabricated SiC nanorods by the carbothermal reduction of sol–gel-derived silica xerogels containing carbon nanoparticles.¹¹ In all cases, the SiC is crystalline with the β -SiC structure (i.e., the 3C polytype^{10–13}). Recently, Zhang et al. synthesized helical SiC/SiO₂ crystalline core–shell nanowires¹⁴ and invoked a screw-dislocation-driven model to explain the growth of the helical β -SiC core.

There are significant differences between the helical SiC nanowires reported by Zhang et al.¹⁴ and helical boron carbide (BC) nanosprings reported by our group.¹⁵ First, the BC nanosprings are amorphous as compared to the crystalline core of the sheathed helical SiC nanowires. Second, the ratio of spring radius to pitch of the BC helices is approximately

unity as compared to 0.20 for the sheathed helical SiC nanowires. In this paper, we report the first observation of single-phase amorphous SiC nanosprings. In addition, we conclusively demonstrate the constraints imposed by crystallinity on the formation of nanosprings. Specifically, a crystalline structure prohibits the formation of near unity radius/pitch ratio nanosprings.

The synthesis of nanowires is promoted through the introduction of a metallic catalyst. This growth mechanism, known as the vapor–liquid–solid (VLS) growth mode, was first described by Wagner and Ellis in 1964.¹⁶ In VLS growth, a liquid droplet of a metal or a metal eutectic resides on a substrate. The droplet absorbs the building block material for the growth of the nanowire from the surrounding vapor. Once the concentration of absorbed material within the droplet reaches supersaturation, the excess material precipitates at the liquid/solid interface, thereby nucleating the nanowire beneath the droplet. VLS can be used to explain not only cylindrical nanowire growth but also complex nanowire structures such as nanosprings.¹⁵

In our previous study of BC nanosprings,¹⁵ we developed a modified VLS model to explain the formation of such structures. In our model, the asymmetry of the growth front arises from contact angle anisotropy (CAA) at the catalyst/nanowire interface, which is derived from the displacement of the center of mass of the spherical catalyst droplet relative to the axis of the as-forming nanowire. This displacement, in turn, results in an imbalance in the surface tension about

* Corresponding author. E-mail: dzhang@uidaho.edu.

the perimeter of the catalyst/nanowire interface. The net nonzero torque acting on the catalyst produces a tumbling-like trajectory about the center axis of the resultant nanospring. The one underlying criterion that must be met in order to realize nanospring growth is that the structure of the nanowire from which the nanospring is formed must be amorphous. Consequently, if a nanowire is crystalline, then the crystalline structure will prohibit such helical growth. The CAA model therefore predicts that nanosprings can be synthesized from any type of material provided they grow by the VLS mode and that they are amorphous.

The SiC nanosprings were grown in a custom-designed parallel plate plasma enhanced chemical vapor deposition (PECVD) chamber operated at 13.56 MHz. Nickel boride (NiB) particles, 100 nm or less in diameter, were used as the catalyst. The NiB was dispersed in ethanol and applied to a cleaned Si substrate. The ethanol solution was allowed to evaporate in air. Because the evaporation rate was moderately slow as well as fairly uniform across the substrate, the catalyst particles were distributed fairly homogeneously across the surface. The precursor for growing SiC nanosprings was *closo*-1,2-dicarbododecaborane ($C_2B_{10}H_{12}$), which is easily sublimated and will be referred to as orthocarborane. The lack of Si in the precursor indicates that the Si substrate acts as the Si source. The orthocarborane provides the carbon. Argon was used as both the carrier gas and the background gas. During the growth process, the Si substrate temperature was maintained at 1050 °C. The source bottle containing orthocarborane was maintained at 60 °C. The Ar gas flow was 5 sccm directly into the PECVD chamber, and an additional 1.5 sccm of Ar passed through the source bottle into the chamber. The chamber pressure was maintained at 122 mTorr: 98 mTorr of Ar and 24 mTorr of orthocarborane/Ar. The plasma power was set to 50 W. The deposition time was 120 min.

The nanowire samples were examined using a Philips CM200 transmission electron microscope (TEM) operated at 200 kV. Sample preparation involved mechanically transferring some of the nanowires from the Si substrate to a carbon-coated copper grid. Alternatively, the nanowires could be dispersed in methanol and then collected, by dipping, on a carbon-coated copper grid. No subsequent thinning was required nor was not necessary to coat the samples with a conductive film for observation in the microscope. Energy dispersive spectroscopy (EDS) was performed using an EDAX system equipped with a detector having an ultrathin polymer window allowing the detection of light elements.

Figure 1 shows two TEM images of segments of two different SiC nanosprings. The diameters of the nanosprings in Figure 1a and b are 75 and 110 nm with nanowire diameters of 37 and 52 nm and pitches of 50 and 70 nm, respectively. This corresponds to radius/pitch ratios of 0.75 and 0.79, respectively. The overall lengths of the nanosprings observed in this study are greater than 1 μ m. Chemical analysis of the nanosprings using EDS indicates that the silicon/carbon ratio is close to 1:1. Selected area diffraction (SAD) patterns of the nanosprings indicate that they are

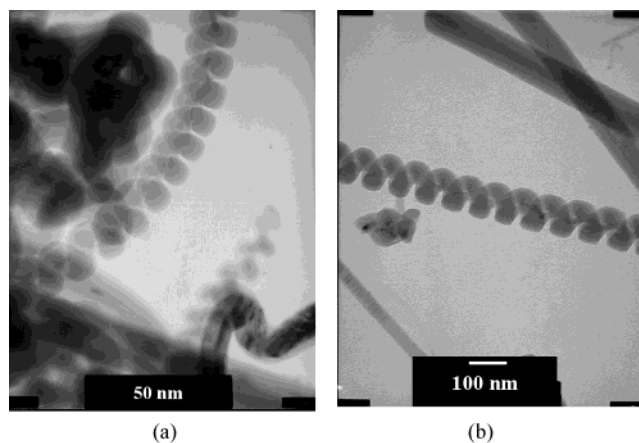


Figure 1. Bright-field TEM images of two amorphous silicon carbide nanosprings.

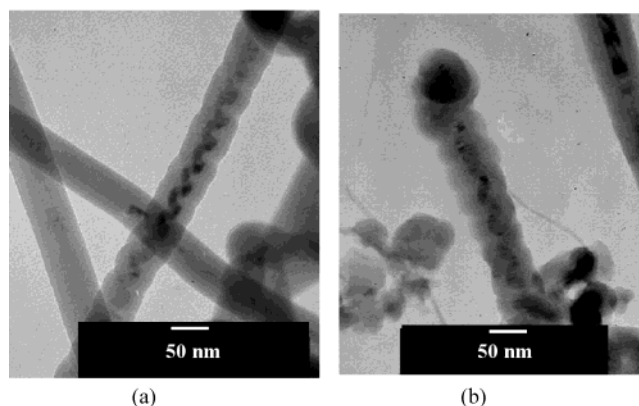


Figure 2. (a) Bright-field TEM image of a biphasic helical SiC nanowire and (b) a TEM image of the NiSi catalyst atop a biphasic helical SiC nanowire.

amorphous. The amorphous structure of the SiC nanosprings is consistent with the requirement for helical growth according to the CAA model.¹⁵

Figure 2 shows two TEM images of biphasic helical SiC nanowires that consist of a crystalline core and an outer amorphous shell. SAD and dark-field imaging were used to determine crystallinity. Located at the end of the helical SiC nanowire in Figure 2b is the metal catalyst that facilitated nanowire formation. This type of nanostructure, a helical crystalline core/amorphous shell, is identical to that found by Zhang et al.¹⁴ In contrast to the results of Zhang et al., EDS analysis of the helix in Figure 2 indicates that both the crystalline core and the outer amorphous shell have an identical chemical composition—1:1 Si/C. The ratio of the radius of the helical core to the pitch of the helix in Figure 2b is 0.26. The presence of the catalyst at the end of the helix in Figure 2b verifies VLS growth. We believe that the coating of the catalyst in Figure 2b with amorphous SiC is indicative of the coformation of the crystalline core and the amorphous shell during VLS growth.

The formation of the biphasic nanowires as opposed to the single-phase structures is poorly understood; consequently, a convincing explanation for this type of growth is lacking. In ref 18, biaxial SiC/SiO₂ nanowires were observed, and their structure was attributed to the minimization of the

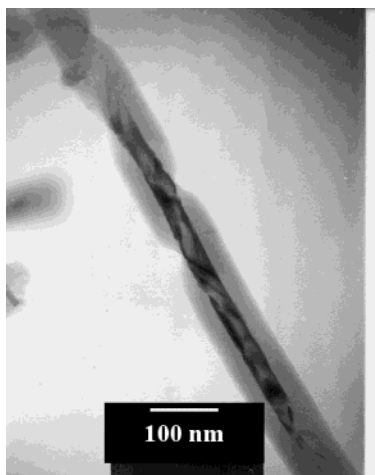


Figure 3. Bright-field TEM image of a silicon carbide amorphous shell spiraling around a SiC crystalline core.

surface free energy associated with defects in the crystalline portion of the nanowire. This explanation is inconsistent with our observation of complex nanowires consisting of amorphous SiC shells that spiral around crystalline SiC cores. An example of one such nanowire is shown in Figure 3. Although the crystalline core does exhibit a high density of defects, the extreme kinking reported for the biaxial SiC/SiO₂ nanowires¹⁸ is not observed. Consequently, we propose an alternative explanation for the formation of complex biphasic nanowires.

The temperature of the catalyst is typically assumed to be uniform. However, there is no evidence to suggest that the temperature of the catalyst must be uniform. As the nanowire grows, the catalyst is lifted off of the surface, at which point it is no longer in direct contact with the heat source. Furthermore, the catalyst cannot be considered to be an adiabatic or isothermal system because of radiative losses, conductive heat transfer with the surrounding vapor, and conduction along the as-forming nanowire. Because the thermal losses take place at the surface of the catalyst, it is reasonable to assume that the temperature at the surface of the catalyst (T_{surface}) is less than the temperature of the core (T_{core}). Whether growth produces crystalline or amorphous structures will depend on the temperature at the liquid–solid interface. We postulate that the lower temperature of the surface of the catalyst reduces the temperature of the liquid–solid interface in the vicinity of the walls of the nanowire. If the temperature at the initiation of nanowire growth is at, or slightly above, a critical temperature for crystalline nanowire formation, then we can envision that the temperature reduction of the liquid–solid interface near the walls of the nanowire will favor amorphous growth and the hotter core will continue to favor crystalline growth. With the condition that $T_{\text{surface}} < T_{\text{core}}$, the diffusion rates near or at the edges of the catalyst will be less than those in the core of the catalyst. The temperature gradient will produce a gradient in the growth rate (J) of the nanowire as a function of the distance from the axis of the nanowire. The growth rate of the nanowire can be approximated by eq 1

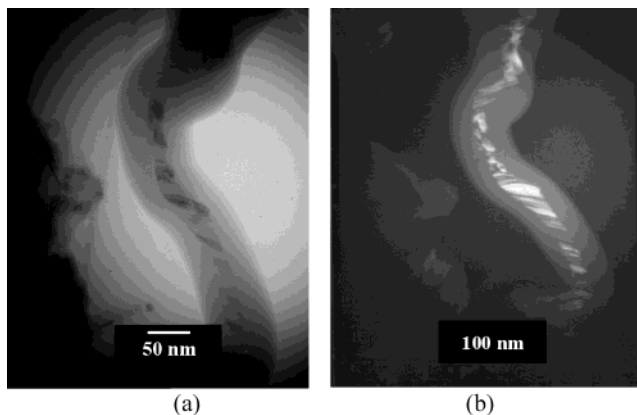


Figure 4. (a) Bright-field and (b) dark-field TEM image of a biphasic SiC nanowire.

$$J = \frac{\alpha \sigma p_o}{\sqrt{2\pi m k T}} \quad (1)$$

where α is the accommodation coefficient, σ is the supersaturation of the vapor, p_o is the equilibrium vapor pressure of the solid at temperature T , m is the molecular mass, and k is the Boltzmann constant.¹⁹ The growth rate is limited by the critical supersaturation specific to the type of growth (i.e., imperfect crystal surface, perfect crystal surface, or clean liquid surface²⁰), where a clean liquid surface is defined as an ideally rough surface consisting of ledges and steps separated only by interatomic distances. The interface between the catalyst and the amorphous shell effectively satisfies this requirement. Note that the critical supersaturation of an imperfect or perfect crystal surface exceeds that of a clean liquid surface. Therefore, under appropriate conditions, the growth rate of the amorphous shell (J_{shell}) would exceed the growth rate (J_{core}) of the crystalline core (imperfect crystal surface). We believe that it is the existence of these competing growth rates in the biphasic SiC nanowire that introduces the necessary fluctuations to induce the helical growth observed in Figure 2.

We propose a model for the helical formation of crystalline nanowires that is based on the CAA model for amorphous nanospring formation. Consider the biphasic SiC nanowire in Figure 4. The formation of this biphasic nanowire is extremely erratic. In particular, the crystalline core exhibits a large number of defects and changes in diameter, but the diameter of the amorphous shell remains essentially constant. In the absence of an amorphous shell, crystalline nanowires are more often than not straight and do not change diameter or exhibit high degrees of disorder, with the exception of stacking faults (particularly common in SiC). The crystalline nanowire in the bottom left corner of Figure 1b is an excellent example of crystalline nanowire formation in the absence of an amorphous shell. On the basis of these observations, it is our opinion that it is the amorphous shell that is driving the distortions in an attempt to steer the nanowire into nanospring growth. We therefore conclude that the highly erratic growth in Figure 4 is due to competition between the amorphous shell and the crystalline core and that the

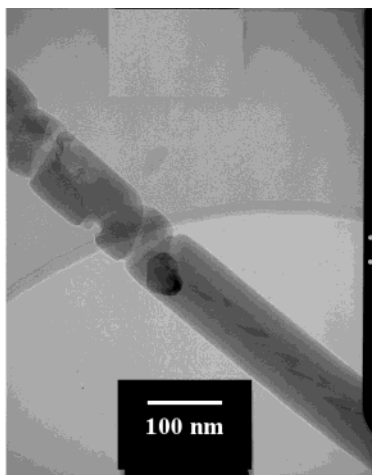


Figure 5. Bright-field TEM image of the transition of a biphasic SiC nanowire to a SiC nanospring.

deformation of the crystalline core is a consequence of this competition.

In support of our hypothesis, we present in Figure 5 a TEM image showing the transition region from straight to helical growth of a SiC nanowire. SAD patterns and dark-field imaging of the nanowire indicate that the straight segment consists of a crystalline core and an amorphous shell and that the helical segment is completely amorphous. Note that at the transition a fraction of the catalyst is embedded at the end of the straight section of the nanowire. On the basis of the CAA model, a portion of the catalyst has been ejected at the point of encapsulation. Similar types of transitions have been observed for BC nanosprings.¹⁵ The significance of the transition in Figure 5 is that nanosprings of the type observed in Figure 1 cannot be achieved in the presence of a crystalline core, which effectively pins the catalyst. We also see from Figure 5 that with the extinction of the crystalline core the pinning of the catalyst is removed and the system can launch into nanospring growth similar to that shown in Figure 1.

The significance of the amorphous shell to the formation of the helical crystalline core of the nanowire in Figure 2 is clarified through the application of the CAA model. Specifically, by analyzing the degrees of anisotropy at the interfaces between the catalyst and the amorphous shell and the catalyst and the crystalline core, we can evaluate the magnitudes of their contributions to the net interfacial anisotropy. In Figure 2b, the diameter of the catalyst (d_{catalyst}) is 68.4 nm, the diameter of the amorphous shell ($d_{\alpha\text{-shell}}$) is 52.6 nm, and the diameter of the crystalline core ($d_{\text{c-core}}$) is 10.5 nm. By offsetting the catalyst from the axis of the nanowire, anisotropy at the point of contact between the catalyst and the nanowire is introduced, and the work of adhesion W of the catalyst to the nanowire is no longer symmetric. The anisotropy of work of adhesion (α_W) can be expressed using eq 2

$$\alpha_W = \frac{W_{\max} - W_{\min}}{W_{\max}} = \frac{\Delta W}{W_{\max}} \quad (2)$$

Using diameters normalized to that of the amorphous shell ($d_{\alpha\text{-shell}}$), we have $d_{\text{catalyst}}/d_{\alpha\text{-shell}}/d_{\text{c-core}} = 1.3:1:0.2$ and an offset between the catalyst and α -shell nanowire ($\Delta_{\text{catalyst}/\alpha\text{-shell}}$) of 0.30. (With this offset, the edge of the amorphous shell of the nanowire is aligned with the edge of the catalyst.) For this geometry, the extrema of the works of adhesions (given in arbitrary relative units) at the catalyst/ α -shell nanowire interface are $W_{\max} = 1.8427 \times 10^{-2}$ and $W_{\min} = 1.0074 \times 10^{-2}$ with $\Delta W = 8.353 \times 10^{-3}$.

Upon inserting these values into eq 2, the anisotropy in the works of adhesions for the amorphous shell $\alpha_W \alpha\text{-shell}$ is

$$\alpha_W \alpha\text{-shell} = \frac{\Delta W}{W_{\max}} = 0.45$$

To evaluate α_W at the catalyst/crystalline core interface, an offset between the catalyst and the crystalline core ($\Delta_{\text{catalyst}/\text{c-core}}$) of 1.5, which is based on the offset used above for the amorphous shell, has been used. Note that the offset for the crystalline core can range from zero to a maximum of 5.5 in normalized dimensions. For an offset of 1.5, the extrema of the works of adhesions for the catalyst/crystalline core interface are $W_{\max} = 1.997 \times 10^{-2}$ and $W_{\min} = 1.923 \times 10^{-2}$ with $\Delta W = 7.4 \times 10^{-4}$.

The corresponding anisotropy in the work of adhesion for the crystalline core $\alpha_W \text{c-core}$ is

$$\alpha_W \text{c-core} = \frac{\Delta W}{W_{\max}} = 0.037$$

The anisotropy in the work of adhesion is clearly dominated by that of the amorphous shell ($\alpha_W \alpha\text{-shell} = 0.45$) relative to that of the crystalline core ($\alpha_W \text{c-core} \approx 0.04$). Furthermore, the anisotropy for the amorphous SiC shell is comparable to that calculated for amorphous BC nanosprings (0.44).¹⁵ From the standpoint of the anisotropy in the works of adhesion of the catalyst to the nanowire, the contribution of the crystalline cores is small; however, we believe that the magnitude of the work of adhesion between the crystalline core and the nanowire is not insignificant. In fact, we propose that the crystalline core effectively pins the catalyst, thereby prohibiting nanospring formation of the type in Figure 1 in favor of helical biphasic formation in Figure 2. The transition from linear to nanospring growth in Figure 5 and the coinciding extinction of the crystalline core at the transition supports our proposition that the crystalline core effectively pins the catalyst and only upon its removal can nanospring formation of the type in Figure 1 occur.

The pinning of the catalyst by the crystalline core is likely a consequence of the fact that nanowire formation is preferential (i.e., the growth direction is along a well-defined crystallographic direction). This direction is often perpendicular to the surface with the minimum free energy. Note that the free energy of the wall of the nanowire should also be taken into account. The net result is that it is energetically unfavorable for the crystalline core to grow in a direction other than that minimizing the free energy. Consequently,

the anisotropy introduced by the amorphous shell acts only as a perturbation during the growth process, with the end result being helical nanowires of the type in Figure 2. The pitch of the amorphous shell/crystalline core helices is likely dictated by the maximum allowable rotation and/or translation vector between adjacent crystal planes. Once again, only with the extinction of the crystalline core can nanosprings of the type in Figure 1 be achieved.

In summary, two distinct types of helical SiC nanowires have been synthesized by PECVD. The first type of helical SiC nanowire, referred to as a nanospring, is single phase and amorphous. These nanosprings have large spring radius-to-pitch ratios of approximately 0.75. The formation of nanosprings can be explained in terms of the CAA model first proposed for the formation of boron carbide nanosprings. The second type of helical SiC nanowire consists of a crystalline core surrounded by an amorphous shell and is referred to as a biphasic helical nanowire. The formation of the biphasic nanowires, linear or helical, has been explained in terms of the existence of temperature gradients within the catalyst. It has been proposed that the temperature near the surface of the catalyst is lower than in the core and that the reduced temperature favors the formation of amorphous material, as opposed to the higher temperature of the core, which favors crystalline growth. In turn, the formation of the helical, biphasic, SiC nanowires is attributed to competition between the growth rates of the two phases. Applying the CAA model for nanospring formation to helical biphasic nanowires, we have demonstrated that the amorphous shell introduces the largest amount of anisotropy. Furthermore, it is argued that the crystal core effectively pins the catalyst, thereby inhibiting nanospring formation in favor of the small radius-to-pitch ratio helices. This conclusion is supported by the observation of a transition of a biphasic SiC nanowire from linear growth to nanospring growth, where at the transition point the crystalline core is annihilated in favor of a single amorphous phase. Future efforts will focus on

the development of heat- and mass-transfer models to describe nanospring formation in detail.

Acknowledgment. We thank Professor D. Eric Aston for his valuable input during the course of writing this manuscript. This work was supported of the W. M. Keck Foundation and the National Science Foundation (EPS-0132626).

References

- (1) Gudixsen, M. S.; Laudon, L. J.; Wang, J.; Smith, D. C.; Lieber, C. M. *Nature* **2002**, *415*, 617.
- (2) Duan, X.; Wang, J.; Lieber, C. M. *Appl. Phys. Lett.* **2000**, *76*, 1116.
- (3) Lee, M. W.; Twu, H. Z.; Chen, C.-C.; Chen, C.-H. *Appl. Phys. Lett.* **2001**, *79*, 3693.
- (4) Schider, G.; Krenn, J. R.; Gotschy, W.; Lamprecht, B.; Ditlbacher, H.; Leitner, A.; Aussenegg, F. R. *J. Appl. Phys.* **2001**, *90*, 3825.
- (5) Adelung, R.; Kipp, L.; Brandt, J.; Tarcak, L.; Traving, M.; Kreis, C.; Skibowski, M. *Appl. Phys. Lett.* **1999**, *74*, 3053.
- (6) Liu, H. I.; Biegelsen, D. K.; Ponce, F. A.; Johnson, N. M.; Pease, R. F. W. *Appl. Phys. Lett.* **1994**, *64*, 1383.
- (7) Alivisatos, P. *Science* **1996**, *271*, 933.
- (8) Wong, E. W.; Sheehan, P. E.; Lieber, C. M. *Science* **1997**, *277*, 1971.
- (9) Wong, K. W.; Zhou, X. T.; Au, F. C. K.; Lai, H. L.; Lee, C. S.; Lee, S. T. *Appl. Phys. Lett.* **1999**, *75*, 2918.
- (10) Dai, H.; Wong, E. W.; Lu, Y. Z.; Fan, S. S.; Lieber, C. M. *Nature* **1995**, *375*, 769.
- (11) Meng, G. W.; Zhang, L. D.; Mo, C. M.; Zhang, S. Y.; Qin, Y.; Feng, S. P.; Li, H. J. *Mater. Res.* **1998**, *13*, 2533.
- (12) Zhou, X. T.; Wang, N.; Lai, H. L.; Peng, H. Y.; Bello, I.; Wong, N. B.; Lee, C. S.; Lee, S. T. *Appl. Phys. Lett.* **1999**, *74*, 3942.
- (13) Hu, J. Q.; Lu, Q. Y.; Tang, K. B.; Deng, B.; Jiang, R. R.; Qian, Y. T.; Yu, W. C.; Zhou, G. E.; Liu, X. M.; Wu, J. X. *J. Phys. Chem. B* **2000**, *104*, 5251.
- (14) Zhang, H. F.; Wang, C. M.; Wang, L. S. *Nano Lett.* **2002**, *2*, 941.
- (15) McIlroy, D. N.; Zhang, D.; Kranov, Y.; Norton, M. Grant. *Appl. Phys. Lett.* **2001**, *79*, 1540.
- (16) Wagner, R. S.; Ellis, W. C. *Appl. Phys. Lett.* **1964**, *4*, 89.
- (17) *Whisker Technology*; Levitt, A. B., Ed.; Wiley-Interscience: New York, 1970; p 249.
- (18) Wang, Z. L.; Dai, Z. R.; Gao, R. P.; Bai, Z. G.; Gole, J. L. *Appl. Phys. Lett.* **2000**, *77*, 3349.
- (19) *Whisker Technology*; Levitt, A. B., Ed.; Wiley-Interscience: New York, 1970; p 69.
- (20) Hirth, J. P.; Pound, G. M. *J. Phys. Chem.* **1960**, *64*, 619.

NL034288C